Ceramics-Silikáty 67 (1), 87-99 (2023)
www.ceramics-silikaty.cz doi: 10.13168/cs.2023.0006

EFFECTS OF DIFFERENT Li_2O/Al_2O_3 RATIOS ON THE STRUCTURE, PHASE COMPOSITION, AND PROPERTIES OF $Li_2O–Al_2O_3–SiO_2$ GLASS-CERAMICS

XIAORONG YANG*, #FENG HE*, **, MINGJUAN SHI*, JUNLIN XIE*, **

*State Key Laboratory of Silicate Materials for Architectures, Wuhan University of Technology, Wuhan, 430070, China
**Faculty of Materials and Manufacturing, Beijing University of Technology, Beijing, 100124, China

#E-mail: he-feng2002@163.com

Submitted January 11, 2023; accepted February 6, 2023

Keywords: Phase composition, Li_2O/Al_2O_3 ratios, Glass-ceramics, Lithium disilicate

In this study, the effects of different Li_2O/Al_2O_3 ratios on the structure, phase composition and properties of $Li_2O–Al_2O_3–SiO_2$ glass-ceramics were investigated. The crystallisation behaviour and structure of the glass samples were investigated using differential scanning calorimetry (DSC), X-ray diffraction (XRD), Fourier transform infrared spectroscopy (FTIR), Raman spectroscopy, field-emission scanning electron microscopy (FE-SEM) and other characterisation methods. When the Li_2O/Al_2O_3 ratio (wt. %) was increased from 0.89 to 2.4, the main crystalline phase changed from quartz to a lithium disilicate (LD) phase, indicating that a high Li_2O/Al_2O_3 ratio (wt. %) was more favourable for the precipitation of the LD phase. Finally, a glass-ceramic with a flexural strength of 199 ± 5 MPa, a microhardness of 767 ± 20 HV and a visible light transmission rate of 80 % at 550 nm was obtained. Owing to its high Li^+ content, this glass-ceramic facilitates chemical strengthening to further improve its mechanical properties and expand its range of applications, such as in electronic display devices.

INTRODUCTION

Glass-ceramics are inorganic non-metallic materials prepared by heat treatment which controls the nucleation and crystallisation processes of glass [1]. They usually comprise one or more crystalline and glass phases and the chief properties primarily depend on the type, distribution, content, and size of the crystal phases [2]. Glass–ceramics possess several excellent properties, such as superior mechanical properties, high chemical durability, adjustable transparency, high thermal stability, and biological activity [3]. Lithium disilicate (LD) is the main crystal phase in $Li_2O–Al_2O_3–SiO_2$ (LAS) glass-ceramics. These types of glass-ceramics possess a higher bending strength and adjustable translucent properties, and is widely used in dental prosthetic materials. These glass-ceramics are new types of materials first developed by Stookey et al. [4] The precipitated crystal phases in LAS photosensitive glass-ceramics are also lithium disilicate and lithium metasilicate; in addition to their mechanical properties, they have good dielectric properties and can be used as substrate materials in integrated circuits and other fields [5].

The high mechanical strength of LD glass-ceramics has been extensively investigated. Hugo R et al. [6] found that chemical stability, densification and other properties can be achieved by adding a small amount of Al_2O_3 and K_2O, and the flexural strength can be increased to 201MPa. Huang et al. [7] successfully fabricated an LD glass-ceramic in a $SiO_2–Li_2O–MgO–Al_2O_3–P_2O_5–ZrO_2$ system with a flexural strength of 562 ± 107 MPa. This is related to the highly-intertwined rod-like interlocking microstructure of the LD crystal phase, which could effectively hinder the fracture propagation and increase the flexural strength of the glass-ceramic. However, for such microstructures, the grain size tends to be too large and can make the glass-ceramic opaque.

The translucency of LD is essential for its application in various fields, which mainly include the field of dental restoration [8-10]. If the transparency of LD glass-ceramics can be improved, it can significantly enhance their potential for application in electronic displays [11]. The transparency of glass-ceramics is largely determined by light scattering, which is influenced by the differences in the relative refractive index and crystal size [12, 13]. LD ceramics are known for their high mechanical strength; however, their large grain size generally results in a loss of transparency. The translucency of LD glass ceramics can be adjusted by altering the size of the LD crystals [14]. Bai et al. [15] investigated the effect of one- and two-step heat treatments on the crystalline phase and microstructure of $Li_2O–SiO_2–Al_2O_3–K_2O–P_2O_5$

glass systems and found that, as compared to the one-step heat treatment, the two-step treatment was more effective in nucleating the LD crystals. Finally, LD glass-ceramics with a grain size of approximately 100 nm were obtained and the actual in-line transmittance measured at 550 nm (d = 2.0 mm) attained a value of 27.3 %, which is significantly greater than that of commercial LD glass-ceramics. Soares et al. [11] prepared a highly translucent nanostructured glass-ceramic by nucleating the parent glass for up to 72 h and subsequently, heating at 660 °C for 2 h. This glass-ceramic was comprised of crystals of a size less than 50 nm as well as a high crystal fraction (52 vol. % $Li_2Si_2O_5$ and 26 vol. % Li_2SiO_3); samples of a size of 1.2 mm exhibited 80 % transparency in the visible spectrum and high flexural strength (350 ± 40 MPa in B3B tests). The results indicate that a longer nucleation time is an important factor for obtaining a sufficiently small crystal size to minimise the loss of light scattering.

Alumina is a typical intermediate oxide in glass-ceramic systems, and Al^{3+} can exhibit a variety of coordination states in oxide glass, resulting in different structural effects. When the alumina content is low, the glass-ceramic of the LAS system is more likely to precipitate the LD phase, whereas, when the alumina content is high, it is easy to precipitate the β-quartz solid-solution phase [16]. Hugo R et al. [6] showed that adding a small amount of Al_2O_3 can improve the mechanical strength and translucency of glass-ceramics. Ananthanarayanan et al. [17] studied the magic-angle spinning nuclear magnetic resonance (MAS-NMR) spectroscopy of several samples with different Li_2O–Al_2O_3 ratios and found that those with a higher Li_2O/Al_2O_3 ratio were more likely to precipitate the LD phase. Leenakul et al. [18] studied the effect of changes in Al_2O_3 content (3-6 mol. %) on the phase formation and mechanical properties of glass-ceramics and reported that as the Al_2O_3 content increases, secondary crystalline phases such as quartz and lithium pyroxene are produced and the mechanical strength decreases. Li_2O is a typical glass network modifier body oxide and Li^+ has the typical characteristics of alkali metal elements, such as low charge, large ion radius, etc. The electric field strengths of Li^+ and O^{2-} are greater because of the smaller force generated. Soares et al. [19] studied the influence of the composition of two different SiO_2/Li_2O ratios (2.39 and 3.39) on their crystallisation behaviour in the SiO_2–Li_2O–K_2O–ZrO_2–P_2O_5 system and found that the LD phase was absent at 900 °C in glass with a higher SiO_2/Li_2O ratio.

The excellent mechanical properties of LD glass-ceramics have been investigated by a number of researchers; however, preparing a transparent LD glass-ceramic with good mechanical properties at the same time is the key problem. Owing to the important roles of Li_2O and Al_2O_3 in the nucleation process and phase composition, in this study, we investigated the effect of different ratios of Li_2O/Al_2O_3 on the structure of the base glass, phase composition and properties of the glass-ceramics to prepare transparent glass-ceramics.

EXPERIMENTAL

Preparation of samples

Base glasses were prepared using pure Li_2CO_3, SiO_2, Al_2O_3, K_2CO_3, $NH_4H_2PO_4$, and ZrO_2 as source materials. SiO_2, Al_2O_3 and Li_2O are the main components of glass, while K_2O can be used as a flux, and P_2O_5 and ZrO_2 can be used as the nucleating agents. Table 1 lists the specific oxide content of the materials. For the preparation of the parent glass, 200 g of the glass mixture was evenly mixed and melted in an alumina crucible in a high-temperature furnace at 1560 °C for 2 h. Pre-heated graphite moulds were then used to form glass blocks of approximately 40 × 40 × 25 mm. Subsequently, the glass was annealed in a muffle furnace at 550 °C for 2 h to eliminate the internal stresses. Finally, using an internal circle cutter, the glass block was sliced into a base glass strip with dimensions of approximately 40 × 4 × 4 mm and subjected to suitable heat treatment to prepare the glass-ceramics. The heat treatment system was determined from the differential scanning calorimetry (DSC) test results.

Sample characterisation

The thermodynamic behaviour of the base glass powder during heating was studied at a rate of 10 °C·min^{-1} using a simultaneous thermal analyser (STA449F3, NETZSCH). Air was used as the test environment, and the test temperature was from ambient temperature to 1000 °C. An X-ray diffractometer (XRD) (D8 Advance, Bruker) was used to identify the type of crystalline phase that precipitated in the glass-ceramics. The local structure of Al^{3+} ions in the base glasses was investigated using a solid-state nuclear magnetic resonance (NMR) spectrometer (Avance III 400 MHz, Bruker) (9.4 T). The ^{27}Al MAS-NMR spectra were recorded at a rotational speed of 12 kHz. Raman spectroscopy of the samples was performed in the range of 300-1600 cm^{-1} using a Raman spectrometer (RM-1000, Renishaw) equipped with an Ar laser. Gaussian solution convolution of the Raman spectra of the parent glass was performed using the Origin software. The infrared (IR) spectra of the glass samples were obtained in the range of 400-1400 cm^{-1} using a Fourier transform infrared (FT-IR) spectrometer (Nicolet 6700, Thermo Electron Scientific Instruments). A Field-electron scanning electron microscope (FE-SEM) (Zeiss Ultra Plus, Zeiss) was used to view the microstructure of the glass-ceramics and the surface of the sample was eroded in a 5 vol. % HF solution for 50 s prior to testing. Measurement of the coefficient of thermal expansion (CTE) of the glass-ceramics was performed with a dilatometer (DIL 402C, NETZSCH) in the range of 30-700 °C at a rate of 10 °C·min^{-1}. The transmittance curves of the glass-ceramics were recorded in the range of 300-800 nm using an ultraviolet-visible-near-infrared (UV-Vis-NIR) spectrophotometer (Lambda 750S, Perkin-Elmer). The thickness of the glass-ceramic samples was

2 mm. Measurements of the mechanical properties of the glass-ceramic samples included the flexural strength and the Vickers hardness (HV). A universal material testing machine (AG-IC50kN, Shimadzu) was used to test the flexural strength of the specimens (40 × 4 × 4 mm) using the three-point bending method. The pivot span and loading speed in this test were set at 25 mm and 9.8 ± 0.1 $n{\cdot}s^{-1}$, respectively. The average flexural strength of each composition was determined by calculating the average flexural strength of five samples with the same composition. A Vickers hardness (HV) tester was used to measure the HV of the samples using a load of 1.96 N and holding time of 10 s. The average microhardness was calculated for each sample with different compositions based on 15 measurements.

RESULTS AND DISCUSSION

Structural analysis of the parent glass

In Figure 1, a broad bun peak representing the glass phase was observed between 20°-30° for samples A1-A5 and the diffraction feature did not appear sharp at any other angles. Thus, the parent glass did not exhibit any signs of crystallisation and predominantly remained in a glass body state dominated by the amorphous phase.

Figure 2 shows the FT-IR absorption spectra of the samples. The shapes of the absorption bands of the samples A1-A5 were essentially the same, as can be observed in Figure 2, with wider absorption bands observed at approximately 467 cm^{-1}, 782 cm^{-1} and 1047 cm^{-1}, and the strongest absorption band occurring in the range of 900-1200 cm^{-1}. As the Li_2O/Al_2O_3 ratio was increased (A1-A5), the peaks of all three absorption bands shifted from higher to lower wavenumbers. Studies have demonstrated that the vibration peak at approximately 467 cm^{-1} is due to the Si–O–Si in-plane bending vibrations within the glass network [20], and a vibration peak at approximately 782 cm^{-1} can be associated with the symmetric stretching vibrations of Si–O–Si and Si–O–Al in the glass network structures [21, 22]. The asymmetric stretching vibrations of Si–O–Si and Si–O–Al in the silicate network can be associated with the vibration peak at approximately 1047 cm^{-1} [23]. The FT-IR spectra of glasses are affected by differences in the bond lengths and bond angles of Si–O–Si owing to the varying degrees of polymerisation of the anionic groups in the silicate network structure. As anion clusters polymerise within this structure, the corresponding IR vibration band shifts towards higher wave numbers. The glass grid structure changes as the Li_2O/Al_2O_3 ratio changes; for instance, the highly polymerised silica-oxygen anion clusters in the silicate network structure decompose into smaller ion clusters, so that the internal density of the glass decreases and the structure becomes looser, ultimately causing the absorption peaks of samples A1-A5 to shift from higher to lower wavenumbers [24].

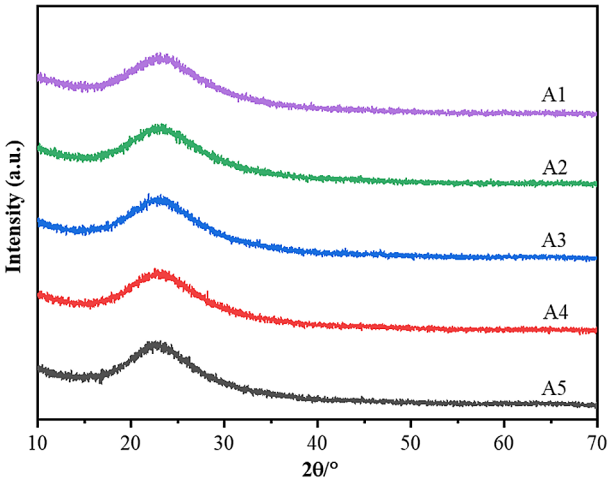

Figure 1. XRD diffraction patterns of the parent glass with different Li_2O/Al_2O_3 ratios.

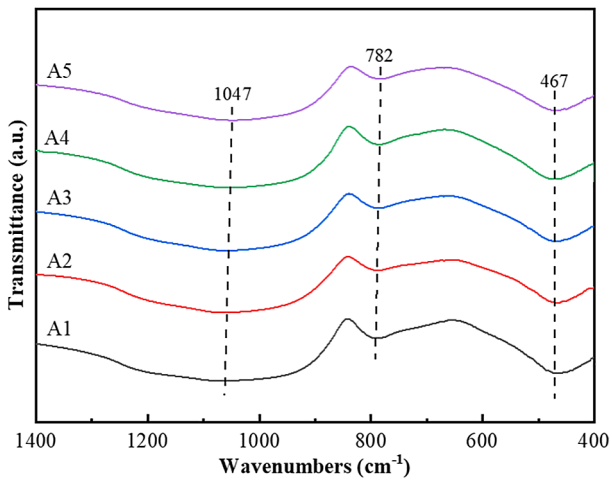

Figure 2. FT-IR patterns of the parent glass with different Li_2O/Al_2O_3 ratios.

Table 1. Composition of the $Li_2O–Al_2O_3–SiO_2$ glass (wt. %).

Composition	SiO_2	Li_2O	Al_2O_3	K_2O	P_2O_5	ZrO_2	Li_2O/Al_2O_3
A1	76.70	8.00	9.00	1.60	1.50	3.20	0.89
A2	76.70	9.00	8.00	1.60	1.50	3.20	1.13
A3	76.70	10.00	7.00	1.60	1.50	3.20	1.43
A4	76.70	11.00	6.00	1.60	1.50	3.20	1.83
A5	76.70	12.00	5.00	1.60	1.50	3.20	2.43

Figure 3 shows the Raman spectra of the parent glass samples A1–A5 with a Raman shift of 200-1600 cm^{-1} and their peak fitting diagrams. It is generally accepted that in silicate glasses, the [SiO_4] tetrahedra are classified into five types based on the number of bridging oxygens, as expressed by Q^n, where n represents the number of

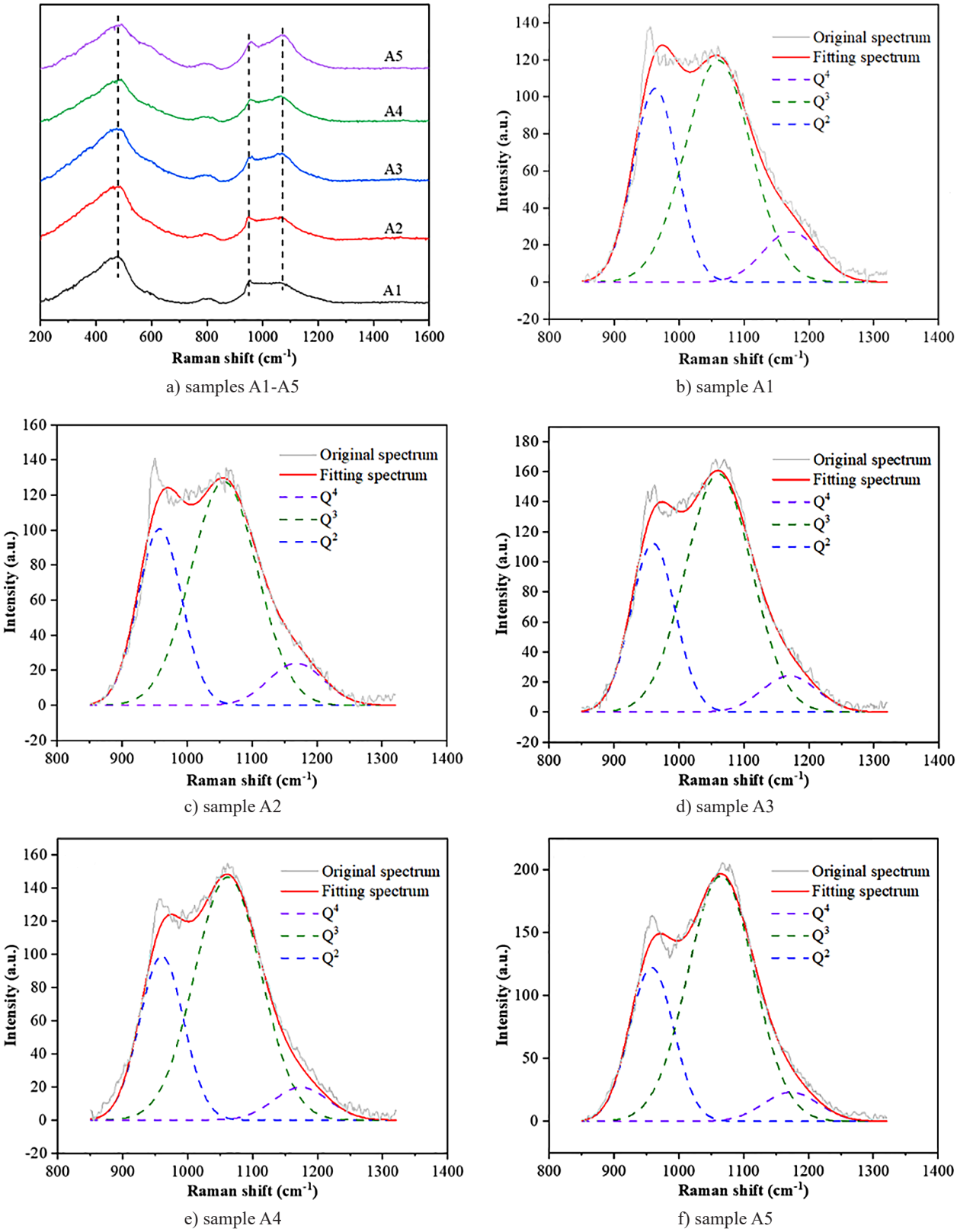

a) samples A1-A5 b) sample A1

c) sample A2 d) sample A3

e) sample A4 f) sample A5

Figure 3. Raman peak fitting patterns of the base glass with different Li_2O/Al_2O_3 ratios: a) sample A1-A5, b) A1, c) A2, d) A3, e) A4, f) A5.

bridging oxygens in each [SiO_4] tetrahedron, and has a value ranging from 0 to 4. The glass network connection degree increases with an increasing n value, resulting in a higher polymerisation degree and a larger Raman shift of the corresponding peak position [17]. The Raman spectra of the parent glass exhibited three distinct broad peaks in the range of 300-600 cm^{-1}, 750-840 cm^{-1} and 900-1200 cm^{-1}. The strong band in the range of 300-600 cm^{-1} can be attributed to the bending vibration (Q^4) of Si–O^0 in the fully polymerised [SiO_4] unit [25, 26] and can be correlated to the symmetric stretching vibrations of Si–O–Si or Si–O–Al in an aluminosilicate glass at 800 cm^{-1} [27], while the band in the range of 900-1200 cm^{-1} corresponds to the asymmetric tensile vibration of Si–O–Si [26]. In the range of 900-1200 cm^{-1}, the peak adjacent to 950 cm^{-1} can be attributed to the asymmetric tensile vibration of Si–O–Si(Q^2) and P–O bond [28, 29], while that closer to 1050 cm^{-1} can be attributed to the asymmetric tensile vibration of Si–O–Si(Q^3) [30]. Figure 3 clearly indicates that with an increasing Li_2O/Al_2O_3 ratio, the peak strength around 1050 cm^{-1} is gradually enhanced, indicating that the quantity of the corresponding groups increases. Therefore, the fitting of the broad peak with a Raman shift of 900-1200 cm^{-1} can be used to semi-quantitatively analyse the polymerisation degree of the glass network. According to some literature, Q^2 is located close to 950 cm^{-1}, Q^3 is near 1050 cm^{-1}, and Q^4 is near 1150 cm^{-1} [28-31]. Figure 4 displays the result of the peak fitting of the parent glass. It can be observed that with an increasing Li_2O/Al_2O_3 ratio, the Q^3 group gradually increased, while the Q^2 and Q^4 groups gradually decreased, indicating that the glass structure gradually becomes loose, which is conducive to the adjustment of the glass structure and the precipitation of specific crystalline phases.

Figure 5 exhibits the ^{27}Al MAS-NMR spectra of the parent glass samples A1-A5 with different Li_2O/Al_2O_3 ratios. The asymmetric peaks in the spectrum are affected by the four-pole coupling of Al. Typical chemical shifts of ^{27}Al MAS-NMR are concentrated at 50-70 ppm for [AlO_4], 30-40 ppm for [AlO_5] and 0-20 ppm for [AlO_6] [32-34]. The ^{27}Al MAS-NMR spectra of all the samples exhibited an asymmetric formant with distinctly similar shapes in the range of 20 to 70 ppm with gradual broadening towards negative values. The main peak in the spectra of all the samples changed only in terms of peak intensity with changes in the Li_2O/Al_2O_3 ratio and there was no appreciable shift in the position or appearance of other shoulder peaks. The resolution of the ^{27}Al MAS-NMR spectrum is poor; therefore, it cannot be simply processed by peak fitting to quantify the different Al coordination polyhedron coordination units. This is consistent with the report that Al is mainly present in the [AlO_4] group and participates in the network structure when $R_2O/Al_2O_3 > 1$ (mol. %) in aluminosilicate glasses [28]. Therefore, a change in the Al_2O_3 content does not significantly change the coordination state of Al^{3+} in the LAS parent glass; Al^{3+} mainly exists in the form of [AlO_4] coordination.

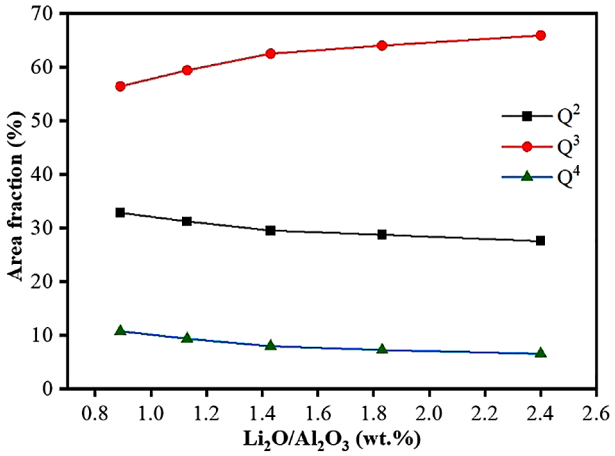

Figure 4. Q^n area fraction of the parent glass with different Li_2O/Al_2O_3 ratios.

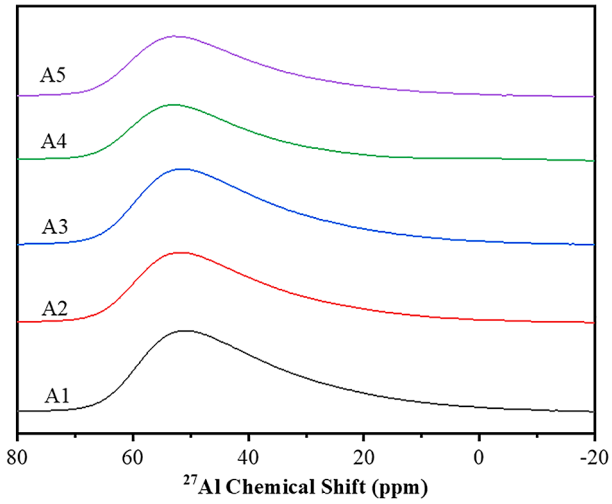

Figure 5. ^{27}Al MAS-NMR spectrum of the parent glass samples A1-A5 with different Li_2O/Al_2O_3 ratios.

Thermal behaviour analysis

The parent glass sample was subjected to thermal analysis testing, by which the characteristic temperature point of the glass can be obtained. A thermodynamic analysis allows a general investigation of the structural changes, crystallisation temperature range and crystalline phase transformation of the base glass, so that the heat treatment regime of the glass can be determined. The parent glasses with different Li_2O/Al_2O_3 ratios were subjected to DSC analysis at a heating rate of 10 °C·min^{-1} under air atmosphere and the corresponding DSC curves are shown in Figure 6. With an increasing Li_2O/Al_2O_3 ratio (wt. %) (A1-A5), the glass transition temperature (T_g) of the parent glass gradually decreased from 553 °C

to 506 °C. This is because, as the ratio of Li_2O/Al_2O_3 increases, the "free oxygen" increases, and the glass network becomes looser, making it easier to restructure the interior of the glass [35]. In addition, the A1 and A2 samples exhibited a wide range of single peaks between 750 and 850 °C; a variety of crystal phases may form in this temperature range and multiple peaks are stacked to form a single wide peak. For samples A3 and A4, two distinct crystallisation peaks were observed, and the first crystallisation peak of A4 was lower than that of A3. This may be owing to the different types of crystalline phases of A5 at high temperatures.

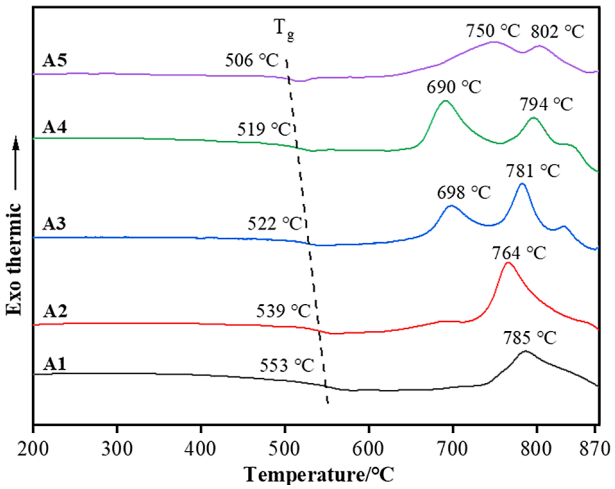

Figure 6. DSC curves of the parent glass with different Li_2O/Al_2O_3 ratios.

Figure 7 shows the CTE test curves of the parent glass samples A1-A5 and the average CTE values in different temperature ranges. As can be observed from Figure 7b), with a change in the Li_2O/Al_2O_3 ratio, the average CTE value in different temperature ranges of the parent glass exhibited a gradual increasing trend. This is because, with an increase in the Li_2O/Al_2O_3 ratio, the glass network structure becomes looser and as the temperature increases, the thermal vibration amplitude of the points in the glass also increases and the distance between the points becomes more spaced, thus exhibiting a gradual increase in the CTE. In particular, we obtained T_g and the softening point temperature (T_s) of the base glass from the thermal expansion test, as shown in Table 2. The T_g value gradually decreased from 543 °C to 494 °C with an increase in the Li_2O/Al_2O_3 ratio (Table 2), which is similar to the results obtained from the DSC.

Combined with the thermal behaviour analysis of the parent glass, the heat treatment system of the glass-ceramic was formulated using a two-step method, as

Table 2. CTE, T_g and T_s of the parent glass with different Li_2O/Al_2O_3 ratios.

α × 10^{-6} (°C)	30-300 °C	30-400 °C	30-500 °C	T_g	T_s
A1	6.389	6.519	6.729	543.3	611.4
A2	6.996	7.196	7.475	530.0	583.3
A3	7.367	7.595	8.077	514.8	572.3
A4	7.637	7.928	8.489	503.4	554.3
A5	8.288	8.544	9.463	494.1	546.5

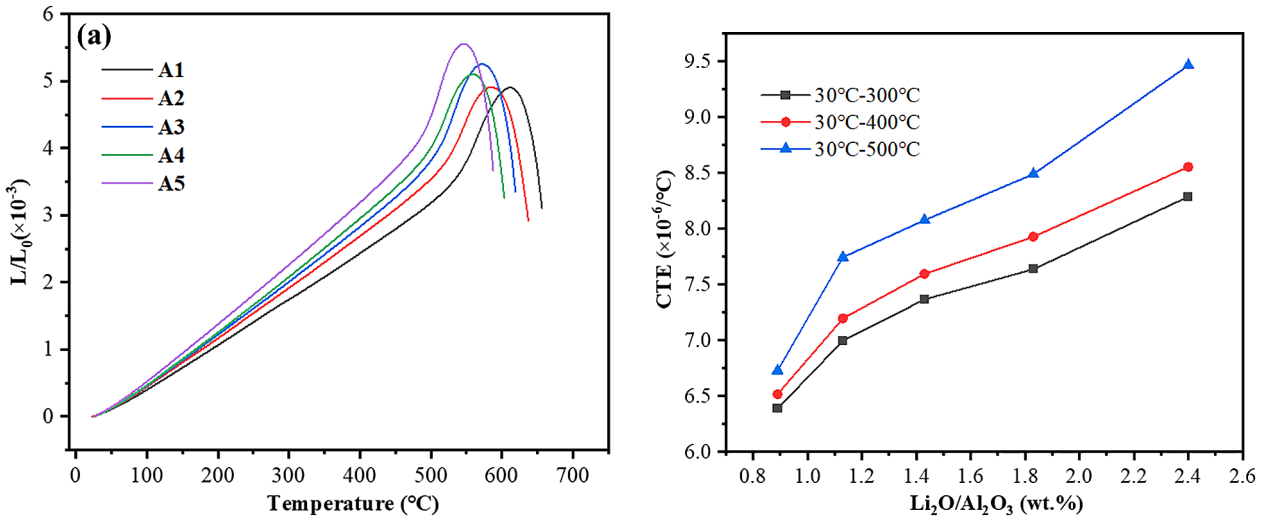

a) CTE test curve

b) Average CTE curve

Figure 7. CTE curves of the parent glass with different Li_2O/Al_2O_3 ratios: a) CTE test curve, b) Average CTE curve with different Li_2O/Al_2O_3 ratios.

shown in Table 3. Furthermore, the nucleation temperature can be defined in the temperature range of T_g and 50 °C above T_g, and the crystallisation temperature can be defined before the crystallisation peak temperature.

Table 3. Heat treatment schemes of the LAS parent glasses.

Nucleation temperature	Dwell time	Crystallization temperature	Dwell time
575 °C	4 h	615 °C	2 h
575 °C	4 h	635 °C	2 h
575 °C	4 h	655 °C	2 h

Structural analysis of the glass-ceramics

The XRD patterns of the glass-ceramic samples at different crystallisation temperatures are shown in Figure 8. Figure 8b shows the XRD pattern of the glass-ceramics at a crystallisation temperature of 615 °C and the precipitated crystal phases are LD ($Li_2Si_2O_5$, ICDD, PDF Number: 40-0376) and lithium monosilicate (LS) (Li_2SiO_3, ICDD, PDF Number: 08-0829). With an increase in the Li_2O/Al_2O_3 ratio, the diffraction peaks of samples A1–A4 gradually became distinct and sharp. The crystallisation degree of sample A5 was low due to the low temperature. Therefore, formation of the LD and LS crystal phases is facilitated by an increase in the Li_2O/Al_2O_3 ratio. Figure 8c shows the XRD patterns at a crystallisation temperature of 635 °C. The variation trend is similar to that at 615 °C. When the crystallisation temperature was increased to 655 °C (Figure 8d), the XRD patterns exhibited a few distinct changes. A sharp peak appeared for sample A1, which can be attributed to the quartz crystals after matching with the standard (quartz, ICDD, PDF Number: 76-1390), while the second phase was permeable lithium feldspar ($LiAlSi_4O_{10}$, ICDD, PDF Number: 75-1716). Quartz crystals can precipitate more easily in the A1 parent glass because they contain more Q^4 groups, while the precipitation of the quartz phase increases the Li-rich and Al-rich phases in the residual glass phase, thus promoting the precipitation of the Li-permeable feldspar phase. With

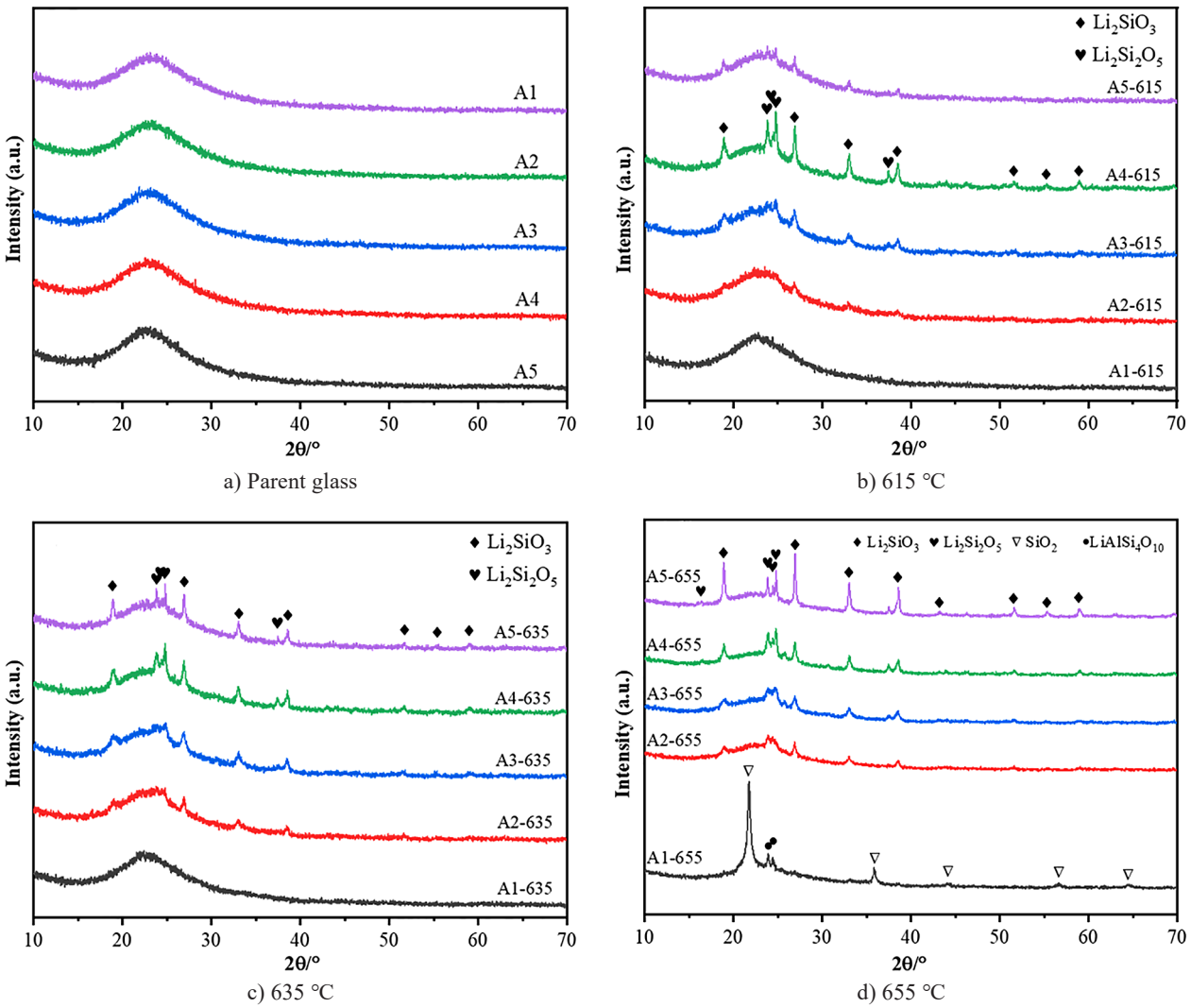

a) Parent glass

b) 615 °C

c) 635 °C

d) 655 °C

Figure 8. XRD diffraction patterns of different Li_2O/Al_2O_3 ratios: a) Parent glass, b) 615 °C, c) 635 °C, d) 655 °C.

an increasing Li_2O/Al_2O_3 ratio, the diffraction peaks of LS and LD in samples A2-A5 were gradually enhanced, indicating that the amount of the crystalline phase also increases. This is because with an increase in the Li_2O/Al_2O_3 ratio, the amount of Q^3 groups in the parent glass increases, which is more beneficial for the precipitation of the LD crystalline phase. The A5 sample exhibited a low diffraction peak and a sudden increase in the strength of the lithium metasilicate peak, which is due to the fact that, at high temperatures, lithium metasilicate is rapidly converted to LD [36, 37].

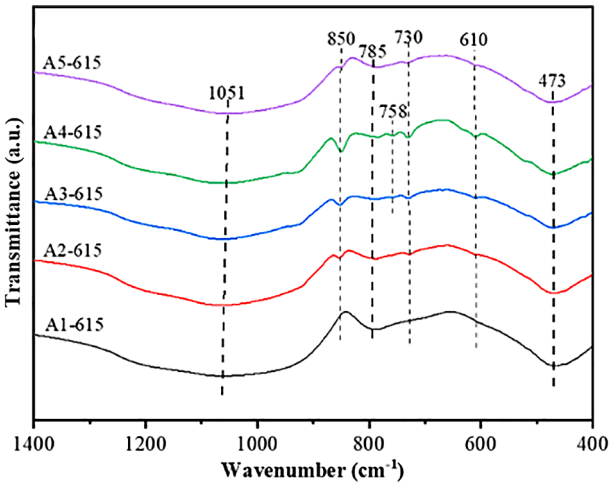

a) 615 °C

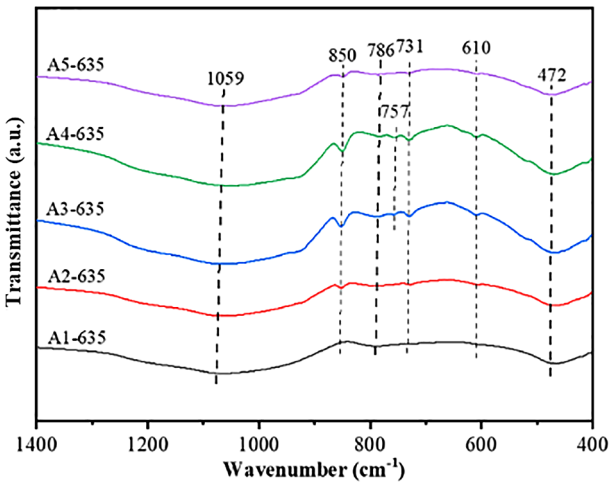

b) 635 °C

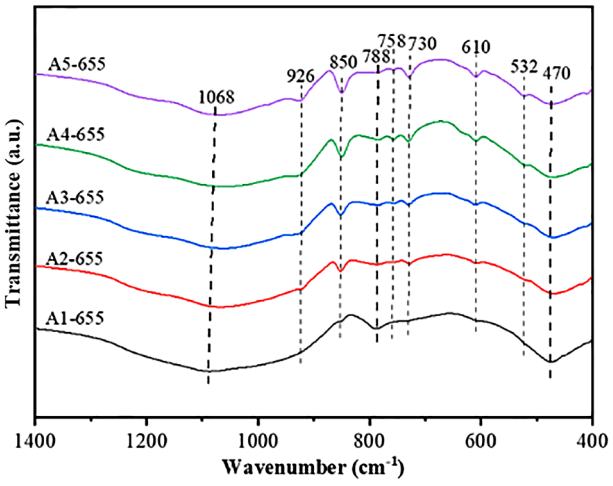

c) 655 °C

Figure 9. FT-IR spectra of the parent glass and glass-ceramics with different crystallisation temperatures: a) 615 °C, b) 635 °C, c) 655 °C.

Figure 9a-c shows the FT-IR curves of the LAS glass-ceramics with different Li_2O/Al_2O_3 ratios. From Figure 9a, it can be observed that the absorption peak band of sample A1 is basically the same as that of its base glass, indicating that sample A1 exhibits no crystallisation. The absorption peak bands of samples A2-A5 were essentially similar in shape and were observed at 472 cm^{-1}, 610 cm^{-1}, 730 cm^{-1}, 758 cm^{-1}, 785 cm^{-1}, 850 cm^{-1} and 1057 cm^{-1}, which are more distinct absorption bands, and the strongest absorption band occurred in the range of 900-1200 cm^{-1}. In contrast to the parent glass, crystals appeared inside the glass-ceramic, causing the IR spectrum to show a few different characteristics. It is clear from Figure 9a and Figure 9b that the spectral band of the glass-ceramic has split, adding four vibrational peaks at 610 cm^{-1}, 730 cm^{-1}, 758 cm^{-1} and 850 cm^{-1}, out of which the one at 758 cm^{-1} is less distinct. The peaks at 610 cm^{-1} and 730 cm^{-1} are attributed to the Si–O–Si symmetric tensile vibration in Li_2SiO_3, while the one at 850 cm^{-1} can be attributed to the Si–O–Si or O–Si–O asymmetric tensile vibration in Li_2SiO_3. The peak at 758 cm^{-1} is attributed to the Si–O–Si symmetric tensile vibration in $Li_2Si_2O_5$ [30, 38]. In Figure 9c, a new absorption band observed at 926 cm^{-1} in the glass-ceramics can be attributed to the asymmetric tensile vibration of Si–O–Si or O–Si–O in $Li_2Si_2O_5$ [30]. In samples A2-A4, the intensity of the absorption gradually increased with a change in the components, which is due to the increasing crystal content. The intensity of the two absorption peaks of A5, 758 cm^{-1} and 921 cm^{-1}, slightly decreased, which is consistent with the XRD analysis results. The FT-IR absorption peaks of the glass-ceramics are provided in Table 4.

Table 4. FT-IR absorption peaks of the glass-ceramics [25-30].

Wave number (cm^{-1})	Vibration types
467	Bending vibration of Si–O–Si
610, 730	Stretching vibrations of Si–O–Si in Li_2SiO_3
755	Stretching vibrations of Si–O–Si in $Li_2Si_2O_5$
784	Stretching vibrations of Si–O–Si
850	Stretching vibrations of Si–O–Si and O–Si–O in Li_2SiO_3
921	Asymmetrical stretching vibrations of Si–O–Si or O–Si–O in $Li_2Si_2O_5$
1060	Asymmetrical stretching vibrations of Si–O–Si or Si–O–Al

Figure 10 shows the Raman spectra of glass-ceramics A1-A5 with different Li_2O/Al_2O_3 ratios, and a new Raman peak was observed. The peak close to 610 cm^{-1} belongs to the stretching vibration or bending vibration (Q^2) of Si–O–Si. The peak at 950 cm^{-1} corresponds to the asymmetric tensile vibration of Si–O–Si(Q^2) and the vibration of the P–O bond, while the peak at 978 cm^{-1} corresponds to the O–Si–O vibration in LS, and the peak at 1105 cm^{-1} corresponds to the Q^3 vibration in LD

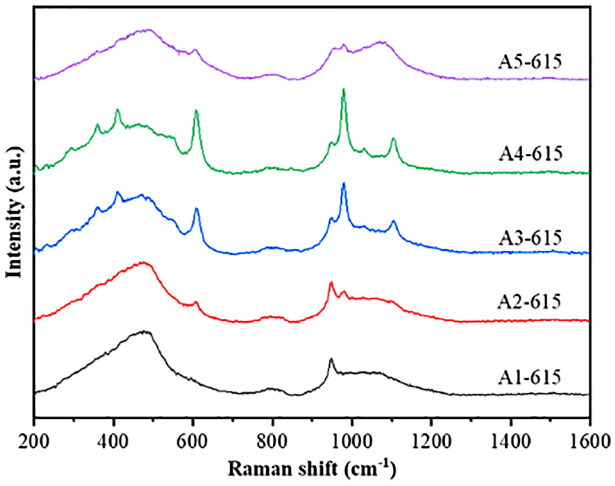

a) 615 °C

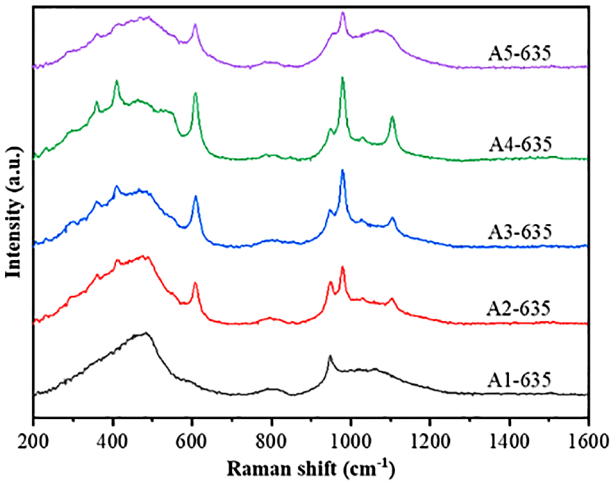

b) 635 °C

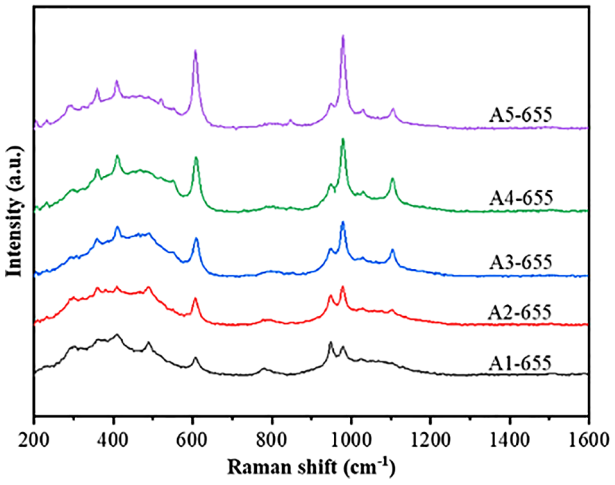

c) 655 °C

Figure 10. Raman spectra of the glass-ceramics with different Li_2O/Al_2O_3 ratios: a) 615 °C, b) 635 °C, c) 655 °C.

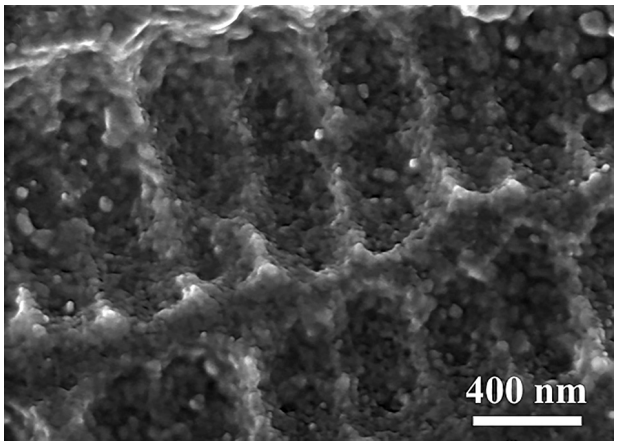

a) A1

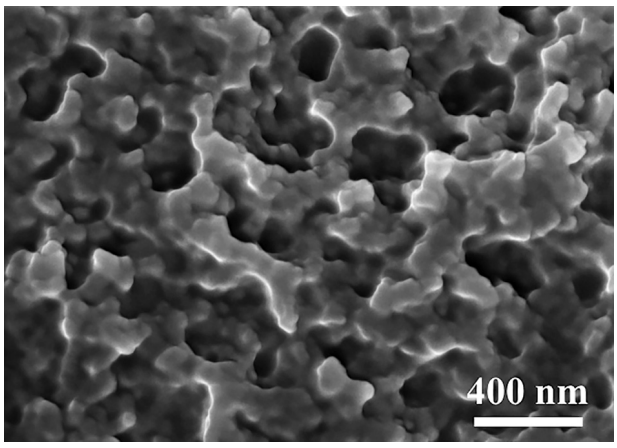

b) A2

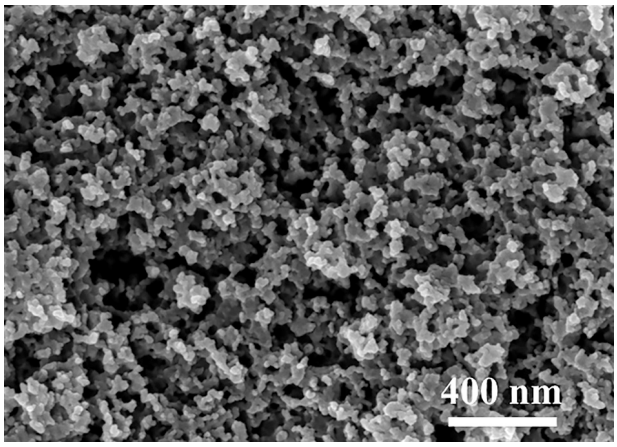

c) A3

Figure 11. SEM images of the glass-ceramics with different Li_2O/Al_2O_3 ratios crystallised at 635 °C for 2 h: a) A1, b) A2, c) A3. *(Continue on next page)*

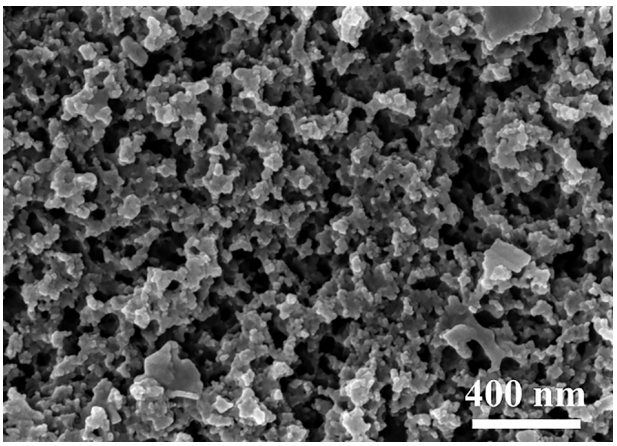

d) A4

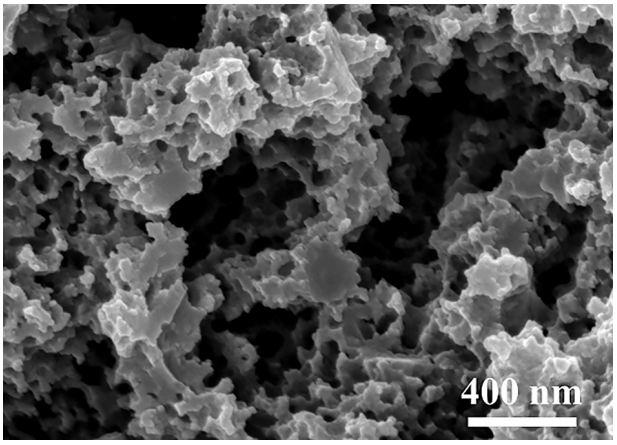

e) A5

Figure 11. SEM images of the glass-ceramics with different Li_2O/Al_2O_3 ratios crystallised at 635 °C for 2 h: d) A4, e) A5.

[30, 38]. At 615 and 635 °C, the Raman spectra of the A1 sample and A1 basic glass were almost unchanged, and the peak intensities at 610 cm^{-1} and 978 cm^{-1} of samples A2-A4 gradually increased with a change in the components. Small peaks at 610 cm^{-1} and 978 cm^{-1} were observed for the A5 sample. These results are consistent with the those of XRD analysis. At 655 °C, the peak intensities at 610 cm^{-1} and 978 cm^{-1} of samples A1-A5 increased gradually with a change in the components, while the peak intensities at 1105 cm^{-1} increased gradually for samples A2-A4, and decreased for sample A5. Sample A1 exhibited a small sharp peak at 480 cm^{-1}, belonging to the Q^4 group, which corresponds to quartz crystal. This is also consistent with the results of XRD analysis.

FE-SEM was used to directly study the morphology, size, and distribution of the crystals in the samples. Figure 11 shows the microstructure of the glass-ceramic samples nucleated at 575 °C for 4 h and crystallised at 635 °C for 2 h. It can be observed that different Li_2O/Al_2O_3 ratios have a remarkable effect on the microstructure of the glass-ceramics, which, in turn, affects their mechanical properties. Figure 11a shows a large depression formed by the erosion of the glass phase. A small number of granular crystals were also be observed in the depression, which may be because the crystal content is too small to be detected by XRD. A small number of larger grains can be observed in Figure 11b; however, the residual glass phase remained as it was not eroded. As shown in Figure 11c, the nucleation density was high; however, large holes still existed. As shown in Figure 11d, the grain size increased and tended to agglomerate with more small pores. As shown in Figure 11e, the grain size increased further and agglomerated into sheets. The eroded glass phase left large pores.

Performance analysis

The degree of crystallisation was lower at a crystallisation temperature of 615 °C and the samples heat treated at a crystallisation temperature of 655 °C showed emulsion formation or loss of transmission. Both of these affected the properties of the glass-ceramics; therefore, the samples of the glass-ceramics at a crystallisation temperature of 635 °C were selected for performance testing. Figure 12 shows the microhardness curves and flexural strengths of the glass-ceramics crystallised at 575 °C for 4 h and at 635 °C for 2 h. It can be observed that with an increase in the Li_2O/Al_2O_3 ratio, the flexural strength of samples A1-A5 gradually increased, with the highest being 213 MPa for A5. Sample A1 was found to contain very few crystals in Figure 11a; hence, the XRD analysis could not detect them. Therefore, sample A1 had the lowest flexural strength. The crystal content of samples A2 and A3 increased with an increase in the Li_2O/Al_2O_3 ratio, and the crystal distribution of A3 samples was dense, which was favourable for improving the mechanical properties. However, a reduction in the flexural strength of sample A4 could be owing to the occurrence of microcracks in the uneven crystallisation, accelerating the crack expansion. The increase in the flexural strength of sample A5 may be owing to the

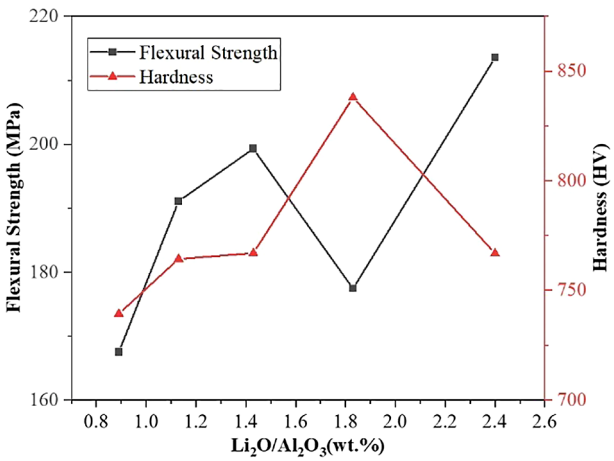

Figure 12. Mechanical properties of the glass-ceramics with different Li_2O/Al_2O_3 ratios crystallised at 635 °C for 2 h.

agglomeration of the grains into sheets, which may be useful in preventing any crack extension, contributing to the enhancement in the flexural properties. The microhardness of the glass-ceramics first increased and subsequently decreased, with a maximum of 838 HV for sample A4, as shown in Figure 12. The increase in the microhardness can be attributed to the increase in the Li_2O/Al_2O_3 ratio, which promotes crystallisation causing the inside of the glass to be more compact. The decrease in the microhardness of the A5 sample was due to the low degree of crystallisation. This is consistent with the XRD results.

Figure 13 shows the CTE curves for different Li_2O/Al_2O_3 ratios of the glass-ceramics. At a crystallisation temperature of 635 °C, the CTE value increased gradually with an increase in the Li_2O/Al_2O_3 ratio, because, at this temperature, the XRD of sample A1 exhibited a steamed bun peak of the amorphous state, indicating that sample A1 is mainly in the glass phase; therefore, the CTE of sample A1 is basically the same as that of the A1 basic glass after heat treatment. The CTE values of samples A2-A5 were slightly lower than that of the basic glass because of the precipitation of LS, the permeability of feldspar, and the LD crystals at this temperature. However, due to the low degree of crystallisation, the glass-ceramics contain more glassy phases, and the CTE value is mainly related to the glassy phase, thus showing an overall gradual increasing trend. The values are listed in Table 5.

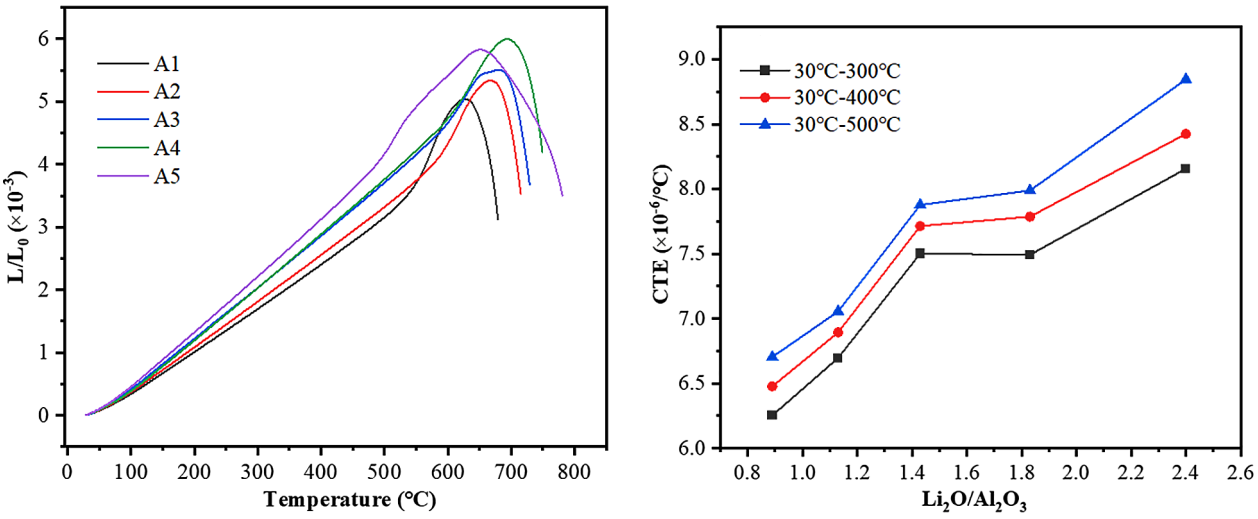

a) CTE test curve b) Average CTE curve

Figure 13. CTE curves of the glass ceramics with different Li_2O/Al_2O_3 ratios crystallised at 635 °C for 2 h: a) CTE test curve, b) Average CTE curve of with different Li_2O/Al_2O_3 ratios.

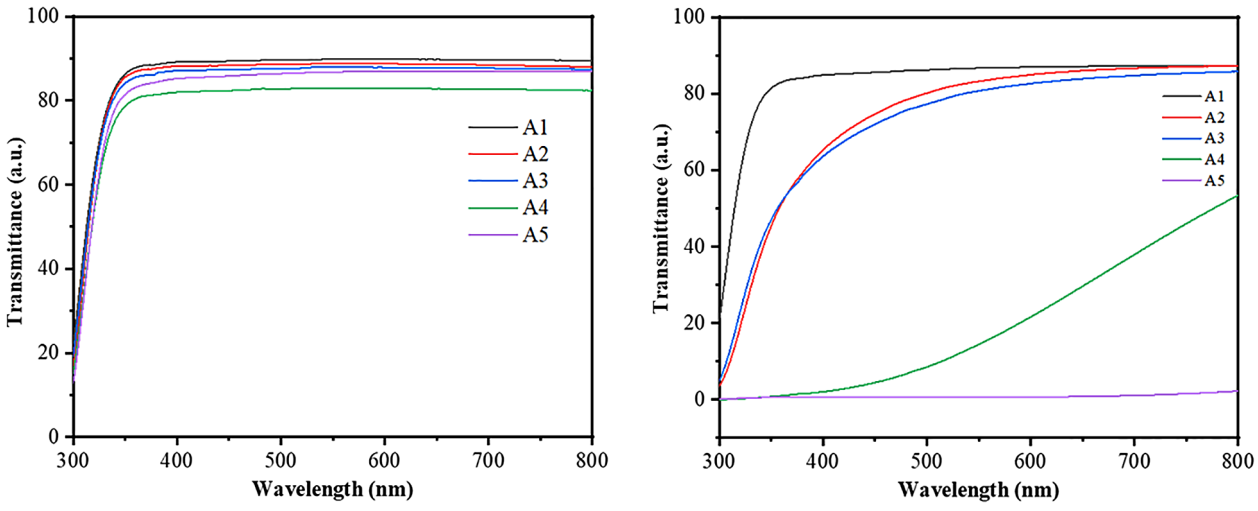

a) parent glass b) glass-ceramics

Figure 14. Transmittance curves in the UV-Vis range (300-800 nm): a) parent glass, b) the glass-ceramics with different Li_2O/Al_2O_3 ratios crystallised at 635 °C for 2 h.

Table 5. CTE of the glass-ceramics with different Li_2O/Al_2O_3 ratios crystallised at 635 ℃ for 2 h.

α×10^{-6} (℃)	30-300 ℃	30-400 ℃	30-500 ℃
A1	6.254	6.478	6.704
A2	6.696	6.894	7.055
A3	7.501	7.713	7.877
A4	7.492	7.785	7.988
A5	8.156	8.424	8.845

The visible light transmittance of the glass-ceramics is affected by defects such as bubbles and stripes, the surface roughness and colour of the glass-ceramics [39].

Figure 14 shows the transmittance curves of the parent glass and glass-ceramics crystallised at 635 °C in the UV-Vis range (300-800 nm). As can be observed in Figure 14a, the visible light transmittance of the parent glass was above 80 %, which may be related to the presence of more bubbles in the parent glass. The transmittances of the glass-ceramics nucleated at 575 ℃ for 4 h and crystallised at 635 ℃ for 2 h are shown in Figure 14b. The transmittance of A1-A3 was approximately 80 % at a wavelength of 550 nm, while that of A4 decreased to approximately 50 %. The decrease in the transmittance of sample A4 is caused by uneven crystallisation. However, the transmittance of sample A5 was as low as 2 %, which appears to be a permeability phenomenon. Combined with the SEM analysis results, this is because the large particles formed by the grain agglomeration led to a large scattering loss so that sample A5 becomes opaque.

CONCLUSIONS

In this study, we investigated the phase formation, structure, and properties of LAS glass–ceramics with different Li_2O/Al_2O_3 ratios. The main conclusions are summarised as follows:

- The glass network structure gradually loosened with an increasing Li_2O/Al_2O_3 ratio (wt. %) (A1–A5), the Q^3 group gradually increased, the Q^2 and Q^4 groups gradually decreased, and the Q^3 group was similar to the LD structure. A change in the Li_2O/Al_2O_3 ratio (wt. %) did not significantly change the coordination state of Al in the basic glass, and most of the Al coordination in all the basic glasses is the [AlO_4] unit.
- When the Li_2O/Al_2O_3 ratio (wt. %) was increased from 0.89 to 2.4, the main crystal phase changed from quartz to the LD phase, implying that a high Li_2O/Al_2O_3 ratio (wt. %) is more conducive to the precipitation of the LD phase.
- When the crystallisation temperature was 635 ℃, with an increase in the Li_2O/Al_2O_3 ratio (wt. %), the CTE of the glass-ceramics also increased, the visible light transmittance gradually decreased, the flexural strength gradually increased, and the microhardness initially exhibited an increasing trend and then decreased. In addition, the comprehensive properties of the A3-635 sample were good: the flexural strength was 199 ± 5 MPa, the microhardness was 767 ± 20 HV, and the visible light transmittance attained a value of 80 % at 550 nm.

Acknowledgment

This work was supported by research fund of Center for Materials Research and Analysis, Wuhan University of Technology (2018KFJJ11). The authors express their sincere gratitude to the Material Research and Testing Center of Wuhan University of Technology.

REFERENCES

1. Holand W., Beall G. H. (2012). Glass–Ceramic Technology, 2nd ed. *John Wiley & Sons*, pp, 75–206.
2. Serbena F. C., Soares V. O., Peitl O., Pinto H., Muccillo R., Zanotto E. D. (2011): Internal Residual Stresses in Sintered and Commercial Low Expansion Li_2O–Al_2O_3–SiO_2 Glass-Ceramics. *Journal of the American Ceramic Society*, *94*, 1206-1214. Doi: 10.1111/j.1551-2916.2010.04220.x
3. Davis M. J., Zanotto E. D. (2017): Glass-ceramics and realization of the unobtainable: Property combinations that push the envelope. *MRS Bulletin*, *42*, 195-199. Doi: 10.1557/mrs.2017.27
4. Stookey S. D. (1959): Catalyzed crystallization of glass in theory and practice. *Industrial and Engineering Chemistry*, *51*, 805-808.
5. Stookey S. D. (1949): Photosensitive glass. *Industrial and Engineering Chemistry*, *41*, 856-861.
6. Fernandes H. R., Tulyaganov D. U., Goel A., Ribeiro M. J., Pascual M. J., Ferreira J. M. F. (2010): Effect of Al_2O3 and K_2O content on structure, properties and devitrification of glasses in the Li_2O–SiO_2 system. *Journal of the European Ceramic Society*, *30*, 2017-2030. Doi:10.1016/j.jeurceramsoc.2010.04.017
7. Huang S., Li Y., Wei S., Huang Z., Gao W., Cao P. (2017): A novel high-strength lithium disilicate glass-ceramic featuring a highly intertwined microstructure. *Journal of the European Ceramic Society*, *37*, 1083-1094. Doi:10.1016/j.jeurceramsoc.2016.10.020
8. Zhang Z., Guo J., Sun Y., Tian B., Zheng X., Zhou M., He L., Zhang S. (2018): Effects of crystal refining on wear behaviors and mechanical properties of lithium disilicate glass-ceramics. *Journal of the Mechanical Behavior of Biomedical Materials*, *81*, 52-60. Doi: 10.1016/j.jmbbm.2018.02.023
9. Gaddam A., Goyal M., Jain S., Bhargava P. (2013): Lithium Disilicate based Glass-Ceramics for Dental Applications. *Transactions of the Indian Ceramic Society*, *72*, 56-60. Doi: 10.1080/0371750x.2013.794027
10. Saint-Jean S. J. (2014*). Dental Glasses and Glass-ceramics*, ed., p.255-277.
11. Soares V. O., Serbena F. C., Oliveira G. d. S., da Cruz C., Muniz R. F., Zanotto E. D. (2021): Highly translucent nanostructured glass-ceramic. *Ceramics International*, *47*, 4707-4714. Doi: 10.1016/j.ceramint.2020.10.039

12. Thiana Berthier V. M. F., Edgar D. Zanotto. (2008): New large grain, highly crystalline, transparent glass–ceramics. *Journal of Non-Crystalline Solids*, *354*, 1721-1730. Doi: 10.1016/j.jnoncrysol.2007.08.052
13. Hendy S. (2002): Light scattering in transparent glass ceramics. *Applied Physics Letters*, *81*, 1171-1173. Doi: 10.1063/1.1499989
14. Jung S. K., Kim D. W., Lee J., Ramasamy S., Kim H. S., Ryu J. J., Shim J. S. (2021): Modulation of Lithium Disilicate Translucency through Heat Treatment. *Materials (Basel)*, *14*, 2094. Doi: 10.3390/ma14092094
15. Bai Y., Peng L., Zhu Q. (2017): The preparation of the lithium disilicate glass-ceramic with high translucency. *Journal of Non-Crystalline Solids*, *457*, 129-134. Doi: 10.1016/j.jnoncrysol.2016.11.032
16. Siligardi C B. L., Bonamartini Corradi A.(2000): Colour development during devitrification in $Li_2O–ZnO–Al_2O_3–SiO_2$ glasses under conventional and microwave heating. *Physics and Chemistry of Glasses*, *41*, 81-88.
17. Ananthanarayanan A., Kothiyal G. P., Montagne L., Revel B. (2010): MAS-NMR studies of lithium aluminum silicate (LAS) glasses and glass–ceramics having different Li_2O/Al_2O_3 ratio. *Journal of Solid State Chemistry*, *183*, 120-127. Doi: 10.1016/j.jssc.2009.10.006
18. Leenakul W., Kraipok A. (2021): Effect of increasing the Al_2O_3 content on the phase formation and mechanical properties of lithium disilicate glass-ceramics. *Materials Research Express*, *8*, 055202. Doi: 10.1088/2053-1591/abffa1
19. Soares R. S., Monteiro R. C. C., Lima M. M. R. A., Silva R. J. C. (2015): Crystallization of lithium disilicate-based multicomponent glasses – effect of silica/lithia ratio. *Ceramics International*, *41*, 317-324. Doi: 10.1016/j.ceramint.2014.08.074
20. Chen M., He F., Shi J., Xie J., Yang H., Wan P. (2019): Low Li_2O content study in $Li_2O–Al_2O_3–SiO_2$ glass-ceramics. *Journal of the European Ceramic Society*, *39*, 4988-4995. Doi: 10.1016/j.jeurceramsoc.2019.07.032
21. Coyle J., Apblett C., Brumbach M., Ohlhausen J., Stoldt C. (2017): Structural and compositional characterization of RF magnetron cosputtered lithium silicate films: From $Li_2Si_2O_5$ to lithium-rich Li_8SiO_6. *Journal of Vacuum Science & Technology A*, 35. Doi: 10.1116/1.4998726
22. Aliyah L. H., Katrina A. T., Hasmaliza M. (2019): Preliminary Study on the Development of New Composition Lithium Aluminosilicate Glass Ceramic. *Materials Today: Proceedings*, *17*, 946-952. Doi: 10.1016/j.matpr.2019.06. 446
23. Shi J., He F., Xie J., Yang H., Guo Z., Liu X. (2019): Exploring the influences of Li_2O/SiO_2 ratio on $Li_2O–Al_2O_3–SiO_2–B_2O_3–BaO$ glass-ceramic bonds for vitrified cBN abrasives. *Ceramics International*, *45*, 15358-15365. Doi: 10.1016/j.ceramint.2019.05.029
24. Kanti Naskar M., Chatterjee M. (2005): A novel process for the synthesis of lithium aluminum silicate powders from rice husk ash and other water-based precursor materials. *Materials Letters*, *59*, 998-1003. Doi: 10.1016/j.matlet.2004.06.075
25. Mozgawa W., Sitarz M. (2002): Vibrational spectra of aluminosilicate ring structures. *Journal of Molecular Structure*, *614*(1-3), 273-279. Doi: 10.1016/S0022-2860(02)00261-2
26. Ross S., Welsch A. M., Behrens H. (2015): Lithium conductivity in glasses of the $Li_2O–Al_2O_3–SiO_2$ system. *Physical Chemistry Chemical Physics*, *17*, 465-74. Doi: 10.1039/c4cp03609c
27. Brawer S. A., White W. B. (1975): Raman spectroscopic investigation of the structure of silicate glasses. I. The binary alkali silicates. *The Journal of Chemical Physics*, *63*, 2421-2432. Doi: 10.1063/1.431671
28. Glatz P., Comte M., Cormier L., Montagne L., Doumert B., Moore G. G. (2018): Different roles of phosphorus in the nucleation of lithium aluminosilicate glasses. *Journal of Non-Crystalline Solids*, *493*, 48-56. Doi: 10.1016/j.jnoncrysol.2018.04.021
29. Mahmoud M. M., Folz D. C., Suchicital C. T. A., Clark D. E., Pinckney L. (2012): Crystallization of Lithium Disilicate Glass Using Microwave Processing. *Journal of the American Ceramic Society*, *95*, 579-585. Doi: 10.1111/j.1551-2916.2011.04936.x
30. Fuss T., Moguš-Milanković A., Ray C. S., Lesher C. E., Youngman R., Day D. E. (2006): Ex situ XRD, TEM, IR, Raman and NMR spectroscopy of crystallization of lithium disilicate glass at high pressure. *Journal of Non-Crystalline Solids*, *352*, 4101-4111. Doi: 10.1016/j.jnoncrysol.2006.06.038
31. Ananthanarayanan A., Kothiyal G. P., Montagne L., Revel B. (2010): MAS-NMR investigations of the crystallization behaviour of lithium aluminum silicate (LAS) glasses containing P_2O_5 and TiO_2 nucleants. *Journal of Solid State Chemistry*, *183*, 1416-1422. Doi: 10.1016/j.jssc.2010.04.011
32. Gambuzzi E., Pedone A., Menziani M. C., Angeli F., Caurant D., Charpentier T. (2014): Probing silicon and aluminium chemical environments in silicate and aluminosilicate glasses by solid state NMR spectroscopy and accurate first-principles calculations. *Geochimica et Cosmochimica Acta*, *125*, 170-185. Doi: 10.1016/j.gca.2013.10.025
33. Stebbins J. F., Kroeker S., Lee S. K., Kiczenski T. J. (2000): Quantification of five-and six-coordinated aluminum ions in aluminosilicate and fluoride-containing glasses by high-field, high-resolution 27Al NMR. *Journal of Non-Crystalline Solids*, *275*(1-2), 1-6. Doi: 10.1016/S0022-3093(00)00270-2
34. Smedskjaer M. M., Youngman R. E., Mauro J. C. (2013): Impact of ZnO on the structure and properties of sodium aluminosilicate glasses: Comparison with alkaline earth oxides. *Journal of Non-Crystalline Solids*, *381*, 58-64. Doi: 10.1016/j.jnoncrysol.2013.09.019.
35. Shan Z., Deng Y., Liu J., Shi F., Liu M., Zhou J., Zhang H., Wu C., Liu T.(2020): Effectively promoting the crystallization of lithium disilicate glass-ceramics by free oxygen in the glass. *Materials Chemistry and Physics*, *240*, 122131. Doi: 10.1016/j.matchemphys.2019.122131
36. Höland W., Apel E., van 't Hoen C., Rheinberger V. (2006): Studies of crystal phase formations in high-strength lithium disilicate glass–ceramics. *Journal of Non-Crystalline Solids*, *352*, 4041-4050. Doi: 10.1016/j.jnoncrysol.2006.06.039
37. Goharian P., Nemati A., Shabanian M., Afshar A.(2010): Properties, crystallization mechanism and microstructure of lithium disilicate glass–ceramic. *Journal of Non-Crystalline Solids*, *356*, 208-214. Doi: 10.1016/j.jnoncrysol.2009.11.015
38. Furukawa T., Fox K. E., White W. B. (1981): Raman spectroscopic investigation of the structure of silicate glasses. III. Raman intensities and structural units in sodium silicate glasses. *The Journal of Chemical Physics*, *75*, 3226-3237. Doi: 10.1063/1.442472
39. Zhou Z., He F., Shi M., Xie J., Wan P., Cao D., Zhang B. (2022): Influences of Al_2O_3 content on crystallization and physical properties of LAS glass-ceramics prepared from spodumene. *Journal of Non-Crystalline Solids*, *576*, 121256. Doi: 10.1016/j.jnoncrysol.2021.121256